Two-dimensional electron gas at the metastable twisted interfaces of CdTe/PbTe (111) single heterojunctions

Shuqiang Jin,[1,*] Chunfeng Cai,[1] Gang Bi,[2] Bingpo Zhang,[1] Huizhen Wu,[1,†] and Yong Zhang[3]

[1]*Department of Physics, State Key Laboratory for Silicon Materials, Zhejiang University, People's Republic of China*

[2]*School of Information and Electrical Engineering, Zhejiang University, City College, People's Republic of China*

[3]*Department of Electrical & Computer Engineering, Optoelectronics Center, University of North Carolina at Charlotte, Charlotte, North Carolina 28223, USA*

(Received 6 January 2013; published 21 June 2013)

The lattice-structure-mismatched CdTe/PbTe heterostructures are emerging materials with unique properties and promising applications in midinfrared optoelectronics and spintronics. High-density two-dimensional electron gas at the metastable twisted interfaces of CdTe/PbTe (111) is investigated experimentally and theoretically. CdTe thin films grown on PbTe(111) using molecular-beam epitaxy are found to have high electron mobilities and carrier concentrations from Hall-effect measurements: 2.02×10^4 cm^2/V s and 4.5×10^{18} cm^{-3} at 2 K, and 6.70×10^3 cm^2/V s and 6.0×10^{19} cm^{-3} at 77 K. Our density-functional theory modeling reveals that the epitaxially grown CdTe/PbTe (111) heterostructures form metastable twisted interfaces that exhibit unusual structural and electronic properties: (1) The PbTe epilayer on CdTe(111) substrates is structurally highly distorted from the rocksalt structure within the first ∼4.5 nm from the interface, which is caused by the stereochemical activity of the Pb s^2 lone pair. (2) The CdTe eplilayer on the PbTe(111) forms spontaneously a high density two-dimensional electron gas (2DEG) over 10^{13} cm^{-2} near the interface, without the need for doping, which explains the experimentally observed high carrier density and mobility. It is a much simpler heterostructure yet able to offer high electron mobility comparable to and one or two order magnitude higher sheet carrier density than the best achieved values for those of Si and II-VI based quantum well structures relying on modulation doping.

DOI: 10.1103/PhysRevB.87.235315 PACS number(s): 68.35.Ct, 68.37.Og, 61.05.jh, 73.20.At

I. INTRODUCTION

Narrow band-gap PbTe is of great interest for its thermoelectric and optical properties and important applications in energy and light sources.[1–4] CdTe/PbTe heterostructures with PbTe in a rocksalt (RS) structure and CdTe in a zinc-blende (ZB) structure have attracted much attention since the PbTe quantum dots (QDs) were demonstrated in a CdTe matrix and shown to exhibit intensively enhanced room-temperature mid-infrared luminescence by Heiss and co-workers.[5] The midinfrared light-emitting diodes with epitaxial PbTe quantum dots embedded in CdTe have been fabricated.[3] A large Rashba splitting has been predicted in CdTe/PbTe/PbSrTe quantum wells (QWs).[6] Recently, we have demonstrated an unusual enhancement of midinfrared light emission due to coupling with surface plasmons in a polar CdTe/PbTe (111) single heterojunction (SHJ).[4] Furthermore, we have found that the CdTe/PbTe (111) interface epitaxially grown on an [111]-oriented substrates is very different from that of PbTe QDs formed by annealing the [100] oriented CdTe/PbTe/CdTe QWs.[7] In the latter case, the crystal planes of the PbTe QDs are all parallel to the corresponding planes of CdTe, which could be viewed as a "natural stacking" of the two different crystalline structures. The structural properties of PbTe/CdTe (100), (110), and (111) interfaces[8] and the electronic properties of the CdTe/PbTe (100) interface have been studied theoretically by Leitsmann and Bechstedt.[9] However, when a CdTe/PbTe heterojunction grows on a [111]-oriented CdTe or PbTe substrate, it instead forms a twisted interfacial structure with new structural properties.[7] By twisted interface we mean that the respective crystal planes of CdTe and PbTe are rotated by 180° with respect to each other about the (111) axis, which results in other crystalline planes of the two materials becoming nonparallel; for instance, the (100) planes on the two sides of the interface are inclined with respect to each other by an angle of 70.6°. We have shown theoretically that the "twisted stacking" is a metastable structure with respect to the "natural stacking" in terms of the total energy, and the formation of the metastable interface is the result of layer-by-layer growth mode,[10] a nonequilibrium process.[7]

Two-dimensional electron gas (2DEG) plays an important role in spintronics and optoelectronics. An extremely long electronic spin lifetime has been observed in the 2DEG in II-VI semiconductors, which could offer the opportunity to coherently manipulate the spin system.[11] High performance transparent biosensors, plasmonic terahertz emitters could be realized by using the high-density and high-mobility 2DEG in ultrashallow single AlN/GaN heterojunctions.[12] In this work, we study the electronic properties of the unusual twisted CdTe/PbTe (111) interface, in particular the formation of a high-density two-dimensional electron gas (2DEG), in a thin CdTe layer near the interface, with an electron mobility and carrier density up to 6700 cm^2/V s and 6.0×10^{19} cm^{-3} at 77 K. This mobility value is substantially higher than that reported for the bulk CdTe 2000 cm^2/V s.[13]

It is known that the RS structure of some IV-VI materials can be distorted by the strong pseudo-Jahn-Teller (PJT) coupling.[14,15] The distorted PbTe RS local structure, which behaves like that in ferroelectrically distorted lone-pair-active Pb^{2+} compounds, such as $PbTiO_3$,[16] was observed by atomic pair distribution function (PDF) analysis at room temperature.[17] It suggests that the RS structure PbTe will

 ©2013 American Physical Society

easily become unstable under certain circumstances. A bulk CdTe crystal is typically an insulator with a wide band gap (∼1.6 eV) in the ZB structure with sp^3 bonding.[18,19] The ZB structure has a peculiar feature along the [111] direction, i.e., the (111) interplanar spacings are alternately wide and narrow. This feature is found to be important in the formation of the unusual metastable CdTe/PbTe (111) interfacial structure.

To explain the formation of the high mobility 2DEG in the CdTe/PbTe (111) SHJ and explore the electronic structures of the twisted interfaces between the two materials, we perform theoretical study on the electronic properties associated with the twisted interfaces using a density-functional theory. Our calculations show that (1) PbTe when grown on (111)-oriented CdTe cannot form the RS structure immediately at the interface but can form a transition structure with alternating interplanar spacings for a few nanometers, thus the electronic properties are significantly changed in the distorted region compared to those of the bulk PbTe. We show that the lattice distortion is caused by the stereochemical activity of the Pb s^2 lone pair,[20,21] as revealed in the orbital resolved density of states (OR-DOS), which drives the two face-center-cubic (fcc) sublattices of the RS structure slightly deviating from each other. (2) The interface between the nanoscale CdTe film and the PbTe(111) substrate forms a very high-density electron gas, which explains the experimentally observed results.

II. THEOTETICAL MODEL

A density-functional theory (DFT) approach within generalized gradient approximation (GGA),[22] implemented in the Vienna *ab initio* simulation package (VASP),[23,24] is applied to study the PbTe/CdTe interface. The spin-orbit coupling (SOC) is taken into account since this effect plays an important role in materials with heavy elements such as Pb and Te.[25] The interaction of the valence electrons with the remaining ions was modeled by pseudopotentials generated within the projector augmented wave (PAW) method.[26] The Cd $4d$ and Pb $5d$ electrons are treated as valence electrons since the outermost occupied d states give rise to the shallow semicore bands which contribute to the chemical bonding in IV–VI materials.[27] The Brillouin zone (BZ) integration is performed by a summation over Monkhorst-Pack special $\boldsymbol{k}$ points.[28] $5 \times 5 \times 1$ $\boldsymbol{k}$ point meshes are used for the vacuum slab modeling.

Since the [111] orientations in both RS-PbTe and ZB-CdTe are polar, the combination of the two slabs leads to a supercell with chemically, structurally, and electrostatically mismatched interface. In the following, the surfaces (interfaces) with the directions of [111] and $[\bar{1}\bar{1}\bar{1}]$ of CdTe are labeled as A (Cd terminated) and B (Te terminated), respectively. The single CdTe/PbTe (111) interfaces are simulated by a dipole corrected stoichiometric slab approximation (D-SA) containing both interfaces A and B to determine the band offset.[8,9] The spurious electric field introduced by the periodic boundary condition results in an artificial electrostatic potential Φ. The difference of its plane average $\Delta\Phi$ between the left- and right-hand sides of a material slab is independent of the slab size. In other words, with increasing the slab thickness, the slope of the artificial dipole potential and thus the resulting nonphysical electrical field diminishes. Therefore we have to construct large supercells to achieve convergence with respect to the atomic displacements at the interface. Meanwhile, a compensating potential that cancels the artificial electric field and an energy correction term are introduced self-consistently in the calculation. 60 layers of the (111) crystal plane are used for CdTe and PbTe, respectively. Two iterations in the self-consistent procedure are performed for the dipole correction. The atomic geometries are allowed to relax until the Hellmann-Feynman forces are smaller than 10 meV/Å. We assume no surface reconstruction, so the slab model contains only one lateral unit cell.

The epitaxial growth of nanoscale CdTe films on the PbTe (111) surface is investigated by the vacuum slab model with a double external field (DEF) correction.[7] In the experimental growth of the materials, the CdTe epitaxial layer is grown on a PbTe buffer layer that is first grown on a BaF_2(111) substrate. However, in the modeling, we consider only a single heterostructure such as CdTe on PbTe, without having to include the BaF_2 substrate, because the buffer layer is usually rather thick (in the order of 1 μm) so that the buffer layer can be treated as the substrate in the modeling. We use 90 layers of the (111) planes to simulate the PbTe substrate. The dangling bonds on the bottom surface are passivated by the pseudohydrogen atoms to remove the influence of the PbTe surface states. For the CdTe (111) thin-film epilayer, 36 atomic layers are used and the upper surface of CdTe is terminated by Te atoms to keep the stoichiometry.

III. RESULTS AND DISCUSSION

A. Interlayer rumpling effect at the twisted interface

We perform a relaxation calculation on the twisted interfaces. The results indicate that the interplanar spacings of PbTe (111) at the interface region become alternately wide and narrow, instead of an equal interplanar spacing (1.87 Å) in the bulk PbTe. We call this an "interlayer rumpling effect" (IRE). Figure 1 shows the interplanar spacings near the interface for $A-$ and $B-$type terminations. The distortion lasts for about 24 atom layers (∼4.5 nm) from the interfaces, i.e., they do not recover to the bulk PbTe structure until more than 24 atomic layers away from interface A or B in the slab. However, the structure of the CdTe does not change much with the largest atom displacement of only 0.02 Å at the interface, and quickly reverts to the bulk structure in four atomic layers.

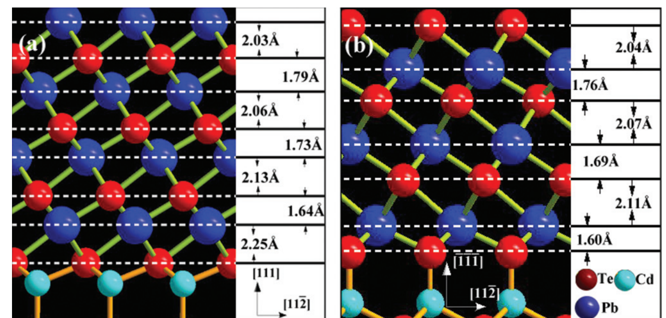

FIG. 1. (Color online) The interplanar spacings of the PbTe (111) layers at (a) the twisted interface A and (b) the twisted interface B.

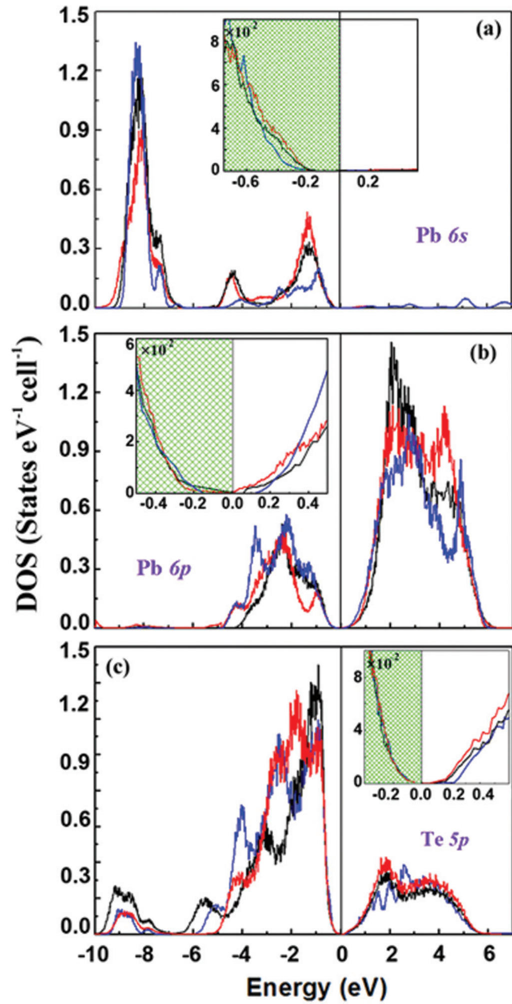

FIG. 2. (Color online) The OR-DOS of the Pb 6s states (a), 6p states (b), and the Te 5p states (c) for bulk PbTe (blue lines), and the PbTe layers (A-P1 and A-C1) at the twisted interface A before relaxation (black lines) and after relaxation (red lines).

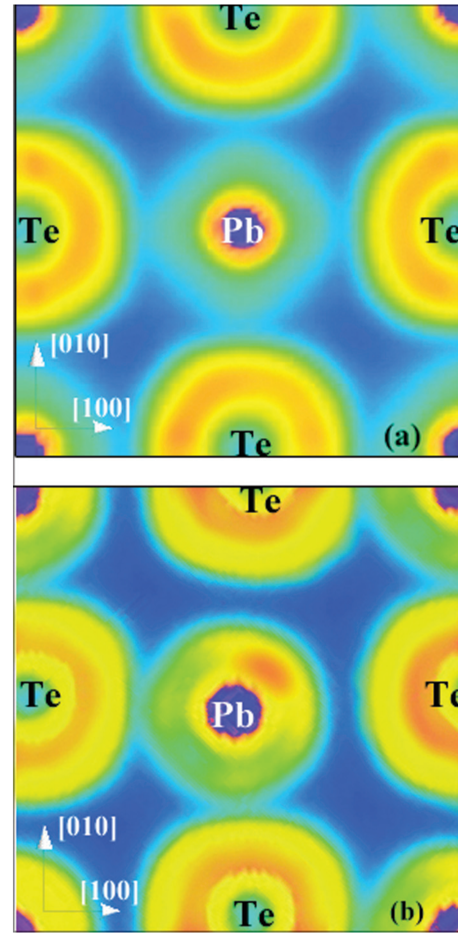

FIG. 3. (Color online) (a) The ELF of 30 layer PbTe away from the twisted interfaces A or B; (b) The ELF of PbTe at the interface A.

B. Density of states at the twisted interface

In order to explore the mechanism of the IRE, we calculated the orbital resolved density of states (OR-DOS). As it is well known from the literature,[29] in the bulk PbTe the Pb 6s states form the lowest but rather narrow band at ∼8 eV below the valence-band maximum (VBM), and a Pb-Te ionic bond mainly consists of Te 5p states and Pb 6p states with some hybridization of Pb 6s states. The DOSs of Pb 6s, 6p and Te 5p states in the bulk PbTe layers are displayed by the blue lines in Figs. 2(a)–2(c), respectively. The RS structure PbTe is stable at 0 K because the s states of the cation participate in the hybridization with a much smaller fraction than that in other IV–VI materials, such as GeS and GeTe in which the crystal structures are more distorted by the s^2 lone pair.[30] However, the OR-DOS of PbTe at the interface is rather different. For convenience, the PbTe and CdTe (111) atomic layers are labeled as $A(B)$-P1, $A(B)$-P2,. . .and $A(B)$-C1, $A(B)$-C2,. . .starting from the interface $A(B)$, respectively. The solid black lines in Fig. 2 illustrate the DOS of Pb s [Fig. 2(a)] and p [Fig. 2(b)] states in the A-P1 layer, and the Te p [Fig. 2(c)] states in the A-C1 layer before the relaxation calculation (in the following discussion, we label these states A-$P1s$, A-$P1p$, and A-$C1p$, respectively). Compared to the corresponding bulk states, a great portion of Pb 6s states transfers from the lowest valence band to the VBM and the s peak at ∼8.0 eV becomes broader, which is similar to the DOS of the GeTe or GeS in a RS structure.[15] The enhanced mixing of s and p orbits of Pb atoms could induce the structural distortion; as a result, RS structure PbTe at the interface becomes unstable, i.e., the stereochemical activity of the Pb s^2 lone pair drives the two fcc sublattices of the RS structure slightly displaced from the ideal positions along [111] direction, which is known as the rhombohedral distortion. In Fig. 2, we plot the DOS of A-$P1s$ (a), A-$P1p$ (b), and A-$C1p$ (c) in red lines after the relaxation calculation. We can see that the displacement of the two fcc sublattices of PbTe weakens the mixing of the p states between Pb and Te atoms while it slightly strengthens the mixing of the Pb s and p states. The mixing between Pb s and p states gradually becomes weaker and weaker when moving further away from the interface.

We have also investigated the electron localization function (ELF)[31] of PbTe near the interfaces. Figure 3(a) shows the ELF of PbTe in the bulk region where the IRE completely disappears. The ELF is almost the same as that in bulk PbTe and the s^2 lone pair is strongly localized in a roughly spherical region around the Pb cations as indicated by the annular orange

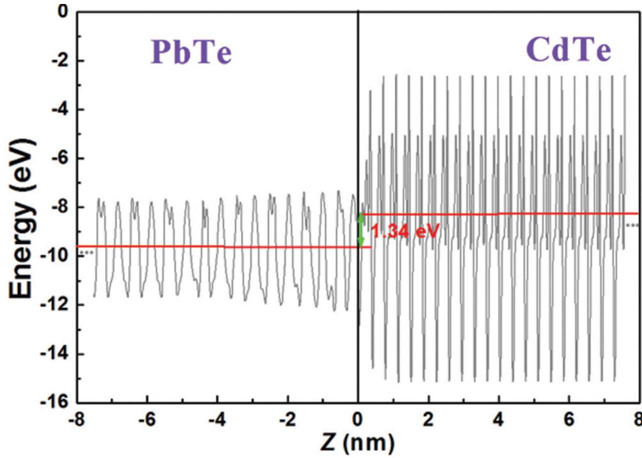

FIG. 4. (Color online) The plane-averaged and the total average ESP for the single interface A.

area centered in the middle of Fig. 3(a). The largely filled Te p shell is also approximately spherical surrounding the Te anions. But the ELF of PbTe at the interface is quite different from that in the bulk PbTe, where the s^2 lone pair gathers to the top right of the Pb cation as illustrated in Fig. 3(b). It is worth mentioning that the s state redistribution phenomenon observed in Fig. 3(b) would not appear if the bulk PbTe lattice was just distorted in the same way as the rhombohedral distortion,[15] which proves that the RS PbTe structure is distorted by the Pb s^2 lone pair at the interface.

C. Band offset of the single PbTe/CdTe(111) interface

We calculate the band offset of a single interface following the procedure of van de Walle and Martin.[32] The major step is to determine the offset between the averaged electrostatic potential (ESP) of PbTe and CdTe [$\Delta\bar{V} = \bar{V}(\mathrm{CdTe}) - \bar{V}(\mathrm{PbTe})$]. As shown in Fig. 4, the thicknesses of the PbTe and CdTe are considered infinity; there is no influence of the electric field induced by the polar interfaces. Because the slab contains both the interface A and B, $\Delta\bar{V}$ gives the same value for the two interfaces. We can see that the lattice structure gradually becomes bulklike as the distance from the interface increases, reflected as the small variation of the plane-averaged ESP curve. The offset between the average ESPs away from the interface ($\Delta\bar{V}$) is 1.34 eV. Using the VBM and the experimentally determined band gaps of PbTe [0.19 eV at 4.2 K,[33] 0.32 eV at 300 K (Ref. 34)] and CdTe [1.6 eV at 4.2 K,[18,19] 1.51 eV at 300 K (Ref. 35)], we obtain the valence-band offset (VBO) and conduction-band offset (CBO) for the twisted (111) interface. As listed in Table I, the calculated VBO of the single interface is smaller than the experimental result measured by the x-ray photoelectron spectroscopy (XPS).[36] Since the XPS can only measure the band offset of HJs formed by growing thin CdTe (PbTe) film on the PbTe (CdTe) (111) surface, the electric field in the polar thin film may influence the experimental result. The CBO is calculated using the band gaps at 4.2 K. Table I also lists the theoretical values of VBO and CBO for the [100] and [110] orientated PbTe/CdTe in the literature.[37] It appears that the theoretical VBO and CBO of the single interfaces do not change much with the interface orientation, and all the three orientations have small VBO values compared to those of CBO. Since PbTe and CdTe have different lattice structures they form different interface structures for different orientations,[8] which causes the small difference of the calculated band offset for different orientations as listed in Table I, where no surface reconstruction is considered in the calculation.

D. Metallic character of CdTe on PbTe (111)

The undoped bulk CdTe is known to be a semi-insulator with a relatively large band gap. However, the polar CdTe/PbTe interface can introduce an intense electric field near the interface, consequently the electronic properties of the CdTe film could be greatly changed.

The CBM of bulk PbTe is at the fourfold degenerate L point. In the case of the CdTe/PbTe (111) heterojunction, the lattice periodicity of PbTe along the [111] direction is broken, which makes the four L points nonequivalent with each other anymore. Figure 5(a) illustrates the calculated band structure of the CdTe/PbTe (111) along the [111] direction. The Fermi energy level is set to be zero. One of the four L points, the longitudinal L point, is folded to the $\bar{\Gamma}$ point; the other three L points (labeled as L') are folded to the $\bar{M}$ points of the 2D BZ that is illustrated in the inset of Fig. 5(b). The difference of the plane-averaged ESP in CdTe ($\Delta\Phi^{\mathrm{CdTe}}$) pulls down the conduction-band edge at the CdTe/PbTe interface. In Fig. 5(a), the valence bands and the unoccupied conduction bands are plotted in blue and green dot lines, respectively. The states illustrated by the red dot lines are the conduction interface states around $1c\Gamma$, cL' and CdTe valence surface states around $v\Gamma$. The yellow conduction band is a partially occupied CdTe bulklike band. Figure 5(b) plots the square of the plane averaged wave functions of a few representative states at the Fermi level, respectively, from the PbTe derived $1c\Gamma$ curve (labeled a), the CdTe derived $2c\Gamma$ curve (b), and the PbTe derived cL' curve (c), and the $v\Gamma$ (valence state), as shown in Fig. 5(a). It appears that states a and c localize mostly in the distorted region of the PbTe side close to the interface, indicating that the distorted region is metallic in nature. However, state b is CdTe derived with the major part of its wave function localized near the interface but on the CdTe side, which indicates that the CdTe thin film also becomes metallic near the interface. The high electron concentration owes to the partially ionized Cd and Pb ions

TABLE I. The band offsets for the PbTe/CdTe interfaces with different orientations.

	Theoretical (111)	Experimental (Ref. 36) (111)	Theoretical (Ref. 37) (110)	Theoretical (Ref. 37) (100)
VBO (eV)	0.030	0.135	0.050	0.000
CBO (eV)	1.380	1.145	1.360	1.410

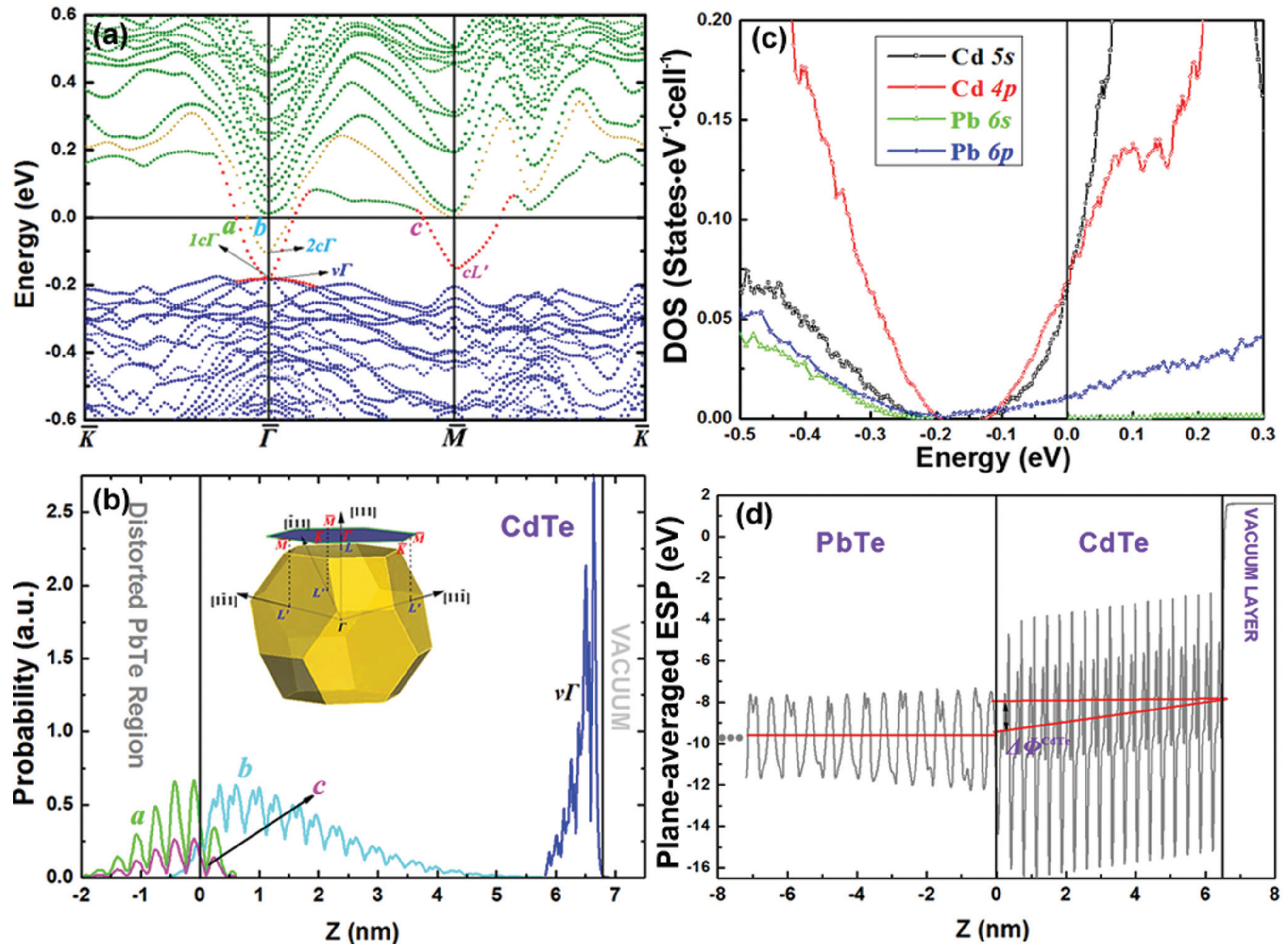

FIG. 5. (Color online) (a) The band structure of the nanoscale CdTe film on the PbTe (111) surface; (b) the plane-averaged wave function squares of the a, b, c, and $v\Gamma$ states labeled in (a), the inset is the 2D BZ; (c) the DOS of the Cd and Pb valence s and p states at the interface A in the CdTe/PbTe (111); (d) the plane-averaged ESP for the interface A formed with a 6.7-nm CdTe film on the PbTe (111) substrate.

at the interface. The DOSs of the Cd and Pb valence s,p states at the interface are plotted in Fig. 5(c), which indicates that the conduction-band electrons mainly come from the Cd $4p$ and $5s$ states of the CdTe film and the Pb $6p$ states of the distorted PbTe region. Figure 5(d) shows the in-plane averaged potential-energy profile for the heterostructure, in particular a band bending of $\Delta\Phi^{\mathrm{CdTe}} = 1.570$ eV on the CdTe side. In conjunction with the wave-function distribution of Figs. 5(b) and 5(d) suggests that the free electrons will tend to accumulate near the interface, thus forming a 2DEG.

In experiment, we grew a series of CdTe/PbTe (111) SHJ samples with different thicknesses of CdTe by molecular-beam epitaxy and then measured the carrier density through Hall measurements at different temperatures. The details for the material growth and structural characterization can be found elsewhere.[4] The individual unintentionally doped PbTe layer always shows p-type conductivity with the hole concentration of $\sim 5 \times 10^{17}$ cm^{-3} whereas a single unintentionally doped CdTe layer grown on BaF_2(111) has n-type conductivity with the electron concentration of $\sim 5 \times 10^{16}$ cm^{-3} which presents rather high resistivity. However, an unintentionally doped nanoscale CdTe layer grown on PbTe (111) is found to have very low resistivity with n-type conductivity. Hall-effect measurements at 300 K show that the electron concentration of CdTe increases exponentially from 1.27×10^{18} cm^{-3} at CdTe thickness of 350 nm to 9×10^{19} cm^{-3} with decreasing the thickness down to 30 nm, as shown in Fig. 6. Although the Hall data only give an average electron concentration of the material probed, it indicates that there is an extremely high density of electrons near the CdTe/PbTe (111) interface. Compared to the bulk CdTe grown by the travelling heater method (THM), in which the mobility is found to be less than 2000 cm^2/V s at 77 K with much lower electron concentration (1.0×10^{16} cm^{-3}),[13] the Hall measurement of the heterostructure sample with 30-nm CdTe shows the highest mobility of 6.70×10^3 cm^2/V s with electron concentration of 6×10^{19} cm^{-3} at 77 K. It is found that the resistivity of the CdTe/PbTe SHJ samples rises remarkably with the thickness increase of the CdTe film. At 300 K, the mobility reduces to 300–400 cm^2/V s, with approximately the same carrier concentration. Although somewhat lower than the reported 300-K bulk value of 1000 cm^2/V s,[13] the carrier concentration is about four orders of magnitude higher. Using the maximum experimental result for the average carrier concentration of 9.0×10^{19} cm^{-3} (at 300 K) and an approximate metallic layer thickness of

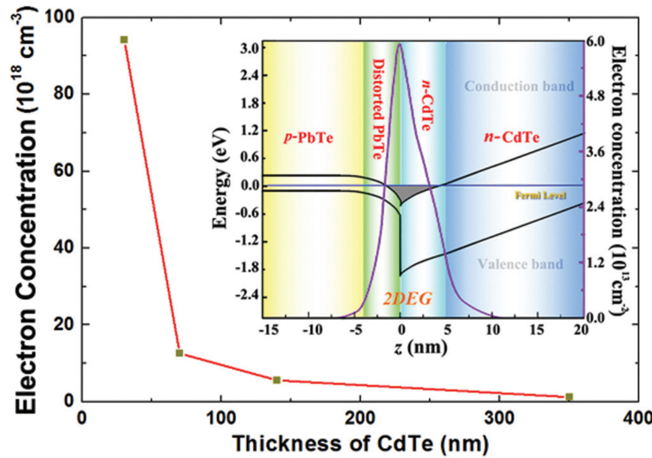

FIG. 6. (Color online) The electron concentrations in the nanoscale CdTe films with different thicknesses measured at 300 K. The inset shows the band profile and the electron density of the CdTe/PbTe HJ calculated by a Schrödinger-Poisson solver.

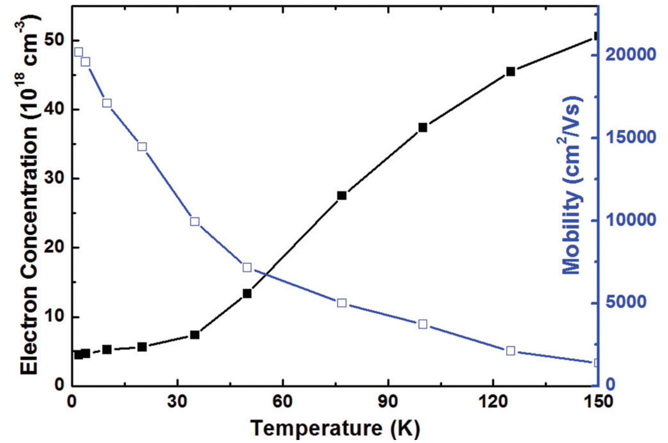

FIG. 7. (Color online) The electron concentrations and mobilities in the CdTe (75 nm)/PbTe (500 nm) SHJ at different temperatures.

$\sim$4 nm estimated from the wave-function extension shown in Fig. 5(b), the 2DEG carrier density is $\sim 3.6 \times 10^{13}$ cm^{-2}.

According to heterojunction theory, the band bending of undistorted PbTe crystal should be very small as PbTe (with hole concentration of $\sim 10^{17}$ cm^{-3}) has a very large dielectric constant of PbTe ($\varepsilon_r^{\mathrm{PbTe}} = 414$). We calculated the band profile and the electron distribution at the heterojunction interface using a combined Schrödinger-Poisson solver and the DFT calculated data discussed above. The effective-mass parameters in the Schrödinger equation is cited from Ref. 6 and an average electron density is set to 3.6×10^{13} cm^{-2} at the interface. We discovered that it is impossible to confine electrons in the distorted PbTe region with such a large dielectric constant of PbTe, no matter what level its background doping is. However, the DFT calculation shown in Fig. 5(b) indicates that this portion of the electrons is confined in the distorted PbTe layer, which implies that the dielectric constant of PbTe near the interface has been changed due to the lattice distortion. Since the PbTe (111) interplanar spacing becomes alternately wide and narrow around the interface which is similar to the lattice of CdTe(111) material, it is rational to assume that the distorted PbTe layer has primarily the same dielectric constant with CdTe ($\varepsilon_r^{\mathrm{CdTe}} = 10.2$). The inset of Fig. 6 shows the calculated band profile diagram and the electron density in the HJ. The electron distribution coincides with the wave function of the states plotted in Fig. 5(b) and the highest electron density at the interface is 5.9×10^{13} cm^{-2}. It is noted that the valence-band offset at the interface is greater than the conduction-band offset which is different from the calculated results listed in Table I for the single interface where it is assumed that the CdTe layer is infinitive and without influence of the electric field induced by the polar interfaces. For the heterojunction formed by covering a thin CdTe layer on PbTe surface, the band bending $\Delta\Phi^{\mathrm{CdTe}}$ lowers the conduction-band minimum of the interface-region CdTe to that below the Fermi level, which causes this region to have a high density of electrons. Due to the large dielectric constant ($\varepsilon_r^{\mathrm{PbTe}} = 414$) and the relatively low carrier density of PbTe, a long space charge region in the PbTe side of the HJ is expected.

Because $\Delta\Phi^{\mathrm{CdTe}}$ does not change with the total thickness of the CdTe film L_{CdTe}, the thickness of the 2DEG in CdTe region increases with L_{CdTe}, which explains qualitatively why the average electron concentration decreases with increasing L_{CdTe}, although it remains above 1.0×10^{18} cm^{-3} when $L_{\mathrm{CdTe}} > 350$ nm. We offer an estimate for the electron concentration by integrating the total charge density of the Cd $5s$, $4p$, and Pb $6p$ states near the interface, which yields a carrier density of the 2DEG as high as 6.0×10^{13} cm^{-2}. Using the maximum experimental result for the average carrier concentration of 9.0×10^{19} cm^{-3} and an approximate metallic layer thickness of $\sim$4 nm estimated from the wave-function extension shown in Fig. 5(b), the 2DEG carrier density is $\sim 3.6 \times 10^{13}$ cm^{-2}, which is rather close to the theoretical estimate.

We also performed the Hall measurement on the CdTe/PbTe (111) SHJ with 75-nm-thick CdTe from 2 to 150 K using a physical property measurement system (PPMS by Quantum Design). As shown in Fig. 7, the electron concentration at 2 K is 4.5×10^{18} cm^{-3} and the mobility is as high as 2.02×10^4 cm^2/V s. As temperature rises, the electron concentration increases while the mobility decreases. At 150 K, the electron concentration reaches 5.1×10^{19} cm^{-3} while the mobility drops to 1.39×10^3 cm^2/V s.

The CdTe/PbTe (111) SHJ bears the similar structural simplicity as well as the performance of AlN/GaN SHJs that also support a 2DEG with high electron mobility up to $\sim$5000 cm^2/V s and a sheet density $\sim 3 \times 10^{13}$ cm^{-2} at 77 K.[12] Compared to those 2DEG structures based on modulation doping, the GaAs/AlGaAs system has been shown to offer higher mobility, for instance $\sim$69 000 cm^2/V s at 77 K, but the sheet density is typically lower ($\sim 5.5 \times 10^{11}$ cm^{-2});[38] the SiGe/Si has achieved somewhat higher mobility of 9000 cm^2/V s but a lower density of 1.0×10^{12} cm^{-2} at 77 K;[39] the ZnCdSe/ZnSe system has achieved a comparable mobility of 7900 cm^2/V s at 4.2 K but the carrier density (5×10^{11} cm^{-2}) is nearly two orders in magnitude lower than our structure.[9] Apparently, the achievable 2DEG carrier density in the QWs with the modulation doping approach tends to be lower than that at the interface of a polarized SHJ such as the previously reported AlN/GaN,[12] and the CdTe/PbTe (111) of this work. In addition, the device structure with modulation

doping is usually significantly more complex. Note that CdTe has substantially larger spin-orbit coupling than CdZnSe (0.95 eV for CdTe vs 0.42 eV for ZnSe),[40] which could be an advantage for the spintronics related properties.

IV. CONCLUSION

We have observed the spontaneous formation of 2DEG at the interface of a thin CdTe layer grown on PbTe (111), and observed high electron mobility through magnetotransport measurement, 2.02×10^4 cm^2/V s at 2 K, 6.70×10^3 cm^2/V s at 77 K, and 300–400 cm^2/V s at 300 K, associated with an extremely high average carrier concentration of 9×10^{19} cm^{-3} or a sheet density of $\sim 3.6 \times 10^{13}$ cm^{-2} (300 K). We performed electronic structure modeling for the metastable twisted CdTe/PbTe (111) polar interfaces using a density-functional theory. Calculations show that the PbTe layer grown on (111) CdTe is not simply a rocksalt structure, but exhibits a distorted region with alternating layer thickness starting from the twisted (111) interface to about 4.5 nm into the PbTe layer. The distortion is caused by the Pb s^2 lone pair according to the calculated orbital resolved density of states. For the structure of CdTe on PbTe (111) substrates, the electronic properties in the distorted interface region and the CdTe film are drastically modified, which leads to the high density 2DEG, as observed experimentally. We also calculated the band offsets between CdTe and PbTe for the (111) heterostructure, giving similar results to those reported in the literature for the (100) and (110) heterostructures. Experimental and theoretical findings of this work suggest a simple heterostructure, a single CdTe/PbTe (111) heterojunction, for supporting a high mobility and high density 2DEG, which opens avenues for future studies and applications of these emerging materials, such as spin manipulation and high-electron-mobility transistors.

ACKNOWLEDGMENTS

This work was supported by National Key Basic Research Program of China (Grant No. 2011CB925603), Natural Science Foundation of China (Grants No. 61290305, No. 91021020, and No. 61275108). The work at UNC-Charlotte was supported by Bissell Distinguished Professorship.

*jinshuqiang@zju.edu.cn
†hzwu@zju.edu.cn

[1] O. Delaire, J. Ma, K. Marty, A. F. May, M. A. McGuire, M.-H. Du, D. J. Singh, A. Podlesnyak, G. Ehlers, M. D. Lumsden, and B. C. Sales, Nat. Mater. **10**, 614 (2011).
[2] T. A. Costi and V. Zlatic, Phys. Rev. Lett. **108**, 036402 (2012).
[3] A. Hochreiner, T. Schwarzl, M. Eibelhuber, W. Heiss, G. Springholz, V. Kolkovsky, G. Karczewski, and T. Wojtowicz, Appl. Phys. Lett. **98**, 021106 (2011).
[4] C. F. Cai, S. Q. Jin, H. Z. Wu, B. P. Zhang, L. Hu, and P. J. McCann, Appl. Phys. Lett. **100**, 182104 (2012).
[5] W. Heiss, H. Groiss, E. Kaufmann, M. Böberl, G. Springholz, F. Schäffler, K. Koike, H. Harada, and M. Yano, Appl. Phys. Lett. **88**, 192109 (2006).
[6] S. Q. Jin, H. Z. Wu, and T. N. Xu, Appl. Phys. Lett. **95**, 132105 (2009).
[7] S. Q. Jin, C. F. Cai, B. P. Zhang, H. Z. Wu, G. Bi, J. X. Si, and Y. Zhang, New J. Phys. **14**, 113021 (2012)
[8] R. Leitsmann, L. E. Ramos, and F. Bechstedt, Phys. Rev. B **74**, 085309 (2006).
[9] R. Leitsmann and F. Bechstedt, Phys. Rev. B **76**, 125315 (2007).
[10] G. Lentz, A. Ponchet, N. Magnea, and H. Mariette, Appl. Phys. Lett. **55**, 2733 (1989).
[11] J. M. Kikkawa, I. P. Smorchkova, N. Samarth, and D. D. Awschalom, Science **277**, 1284 (1997).
[12] Y. Cao and D. Jena, Appl. Phys. Lett. **90**, 182112 (2007).
[13] K. Suzuki, S. Seto, T. Sawada, and K. Imai, IEEE Trans. Nucl. Sci. **49**, 1287 (2002).
[14] O. B. Maksimenko and A. S. Mishehenko, Solid State Commun. **92**, 797 (1994).
[15] U. V. Waghmare, N. A. Spaldin, H. C. Kandpal, and Ram Seshadri, Phys. Rev. B **67**, 125111 (2003).
[16] G. H. Kwei, S. J. L. Billinge, S.-W. Cheong, and J. G. Saxton, Ferroelectrics **164**, 57 (1995).
[17] Emil S. Božin, Christos D. Malliakas, Petros Souvatzis, Thomas Proffen, Nicola A. Spaldin, Mercouri G. Kanatzidis, and Simon J. L. Billinge, Science **330**, 1660 (2010).
[18] Ching-Hua Su, J. Appl. Phys. **103**, 084903 (2008).
[19] B. Segall, M. R. Lorenz, and R. E. Halsted, Phys. Rev. **129**, 2471 (1962).
[20] A. F. Wells, *Structural Inorganic Chemistry*, 4th ed. (Oxford University Press, Oxford, 1974).
[21] B. G. Hyde and S. Andersson, *Inorganic Crystal Structures* (Wiley, New York, 1989).
[22] J. P. Perdew, A. Ruzsinszky, G. I. Csonka, O. A. Vydrov, G. E. Scuseria, L. A. Constantin, X. Zhou, and K. Burke, Phys. Rev. Lett. **100**, 136406 (2008).
[23] G. Kresse and J. Furthmüller, Comput. Mater. Sci. **6**, 15 (1996).
[24] G. Kresse and J. Furthmüller, Phys. Rev. B **54**, 11169 (1996).
[25] D. Hobbs, G. Kresse, and J. Hafner, Phys. Rev. B **62**, 11556 (2000).
[26] G. Kresse and D. Joubert, Phys. Rev. B **59**, 1758 (1999).
[27] S.-H. Wei and A. Zunger, Phys. Rev. B **37**, 8958 (1988).
[28] H. J. Monkhorst and J. D. Pack, Phys. Rev. B **13**, 5188 (1976).
[29] S.-H. Wei and A. Zunger, Phys. Rev. B **55**, 13605 (1997).
[30] G. Bissert and K. F. Hesse, Acta Crystallogr. Sect. B **34**, 322 (1978).
[31] B. Silvi and A. Savin, Nature (London) **371**, 683 (1994).
[32] C. G. Van de Walle and R. M. Martin, Phys. Rev. B **35**, 8154 (1987).
[33] P. Dziawa, B. Taliashvili, W. Domuchowski, L. Kowalczyk, E. Lusakowska, A. Mycielski, V. Osinniy, and T. Story, Phys. Status Solidi C **2**, 1167 (2005).

[34] B. B. Weng, H. Z. Wu, J. X. Si, and T. N. Xu, Chin. Phys. Lett. **25**, 3334 (2008).
[35] R. G. Dhere, Y. Zhang, M. J. Romero, S. E. Asher, M. Young, B. To, R. Noufi, and T. A. Gessert, in *Investigation of Junction Properties of CdS/CdTe Solar Cells and Their Correlation to Device Properties*, Photovoltaic Specialists Conference, 2008. PVSC '08. 33rd IEEE, 11–16 May (IEEE, New York, 2008), pp. 1–5.
[36] J. X. Si, S. Q. Jin, H. J. Zhang, P. Zhu, D. J. Qiu, and H. Z. Wu, Appl. Phys. Lett. **93**, 202101 (2008).
[37] R. Leitsmann, L. E. Ramos, F. Bechstedt, H. Groiss, F. Schäffler, W. Heiss, K. Koike, H. Harada, and M. Yano, Appl. Surf. Sci. **254**, 397 (2007)
[38] S. Hiyamizu, T. Mimura, T. Fujii, K. Nanbu, and H. Hashimoto, Jpn. J. Appl. Phys. **20**, L245 (1981).
[39] K. Ismail, B. S. Meyerson, and P. J. Wang, Appl. Phys. Lett. **58**, 2117 (1991).
[40] O. Madelung, *Semiconductors: Data Handbook*, 3rd ed. (Springer-Verlag, Berlin, 2004).